Supplementary Information for

Cu-exchanged hydroxyapatites as green catalysts for CO oxidation

Guillermo Escolano-Casado[a], Sadaf Fatima Jafri[a], Matteo Signorile[a], Elisa Borfecchia[a] and Lorenzo Mino[a]*

[a]Department of Chemistry and Interdepartmental NIS Centre, University of Torino, Via P. Giuria 7, 10125 Torino, Italy.

*Corresponding author e-mail: lorenzo.mino@unito.it

Table S1. Molar concentration of the $Cu(NO_3)_2$ solution employed for the ion exchange, elemental weight percent (wt.%) composition measured by ICP-OES, atomic ratios and BET specific surface area (SSA) for all Needle and Plate samples.

Sample	$[Cu(NO_3)_2]$ (M)	$[Ca^{2+}]$ wt.%	$[Cu^{2+}]$ wt.%	[P] wt.%	(Ca+Cu)/P	SSA
Needle	-	35.6 ± 0.8	-	15.5 ± 0.3	1.78 ± 0.04	104
Needle_4	0.02	32.3 ± 1.4	3.9 ± 0.2	15.1 ± 0.7	1.78 ± 0.02	98
Needle_6	0.05	31.6 ± 1.0	6.1 ± 0.2	15.3 ± 0.5	1.79 ± 0.01	101
Needle_6'	0.10	30.3 ± 1.0	6.3 ± 0.2	14.8 ± 0.8	1.79 ± 0.02	98
Needle_6''	0.20	29.7 ± 1.0	6.5 ± 0.1	14.5 ± 0.7	1.80 ± 0.02	93
Plate	-	33.16 ± 0.06	-	17.29 ± 0.07	1.48 ± 0.01	199
Plate_4	0.02	30.4 ± 0.4	4.06 ± 0.07	17.1 ± 0.2	1.49 ± 0.01	210
Plate_11	0.05	25.75 ± 0.14	10.75 ± 0.05	16.5 ± 0.2	1.52 ± 0.01	205
Plate_14	0.10	23.3 ± 0.2	14.0 ± 0.2	15.36 ± 0.08	1.62 ± 0.01	192
Plate_14'	0.20	23.5 ± 0.2	14.7 ± 0.2	15.7 ± 0.2	1.61 ± 0.01	170

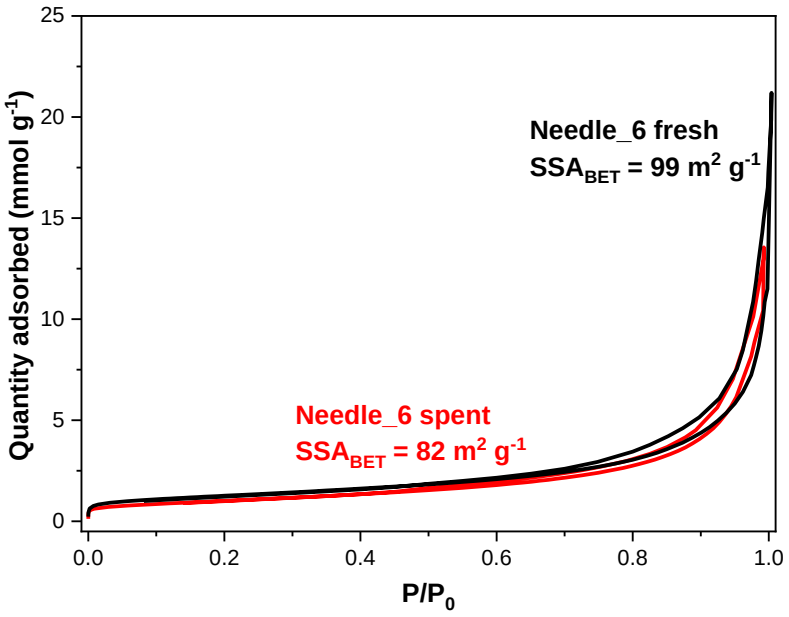

Figure S1. N_2 adsorption-desorption isotherms at 77 K for fresh (as prepared) and spent (after catalytic tests) Needle_6 samples. The corresponding specific surface areas obtained applying the BET model are also reported.

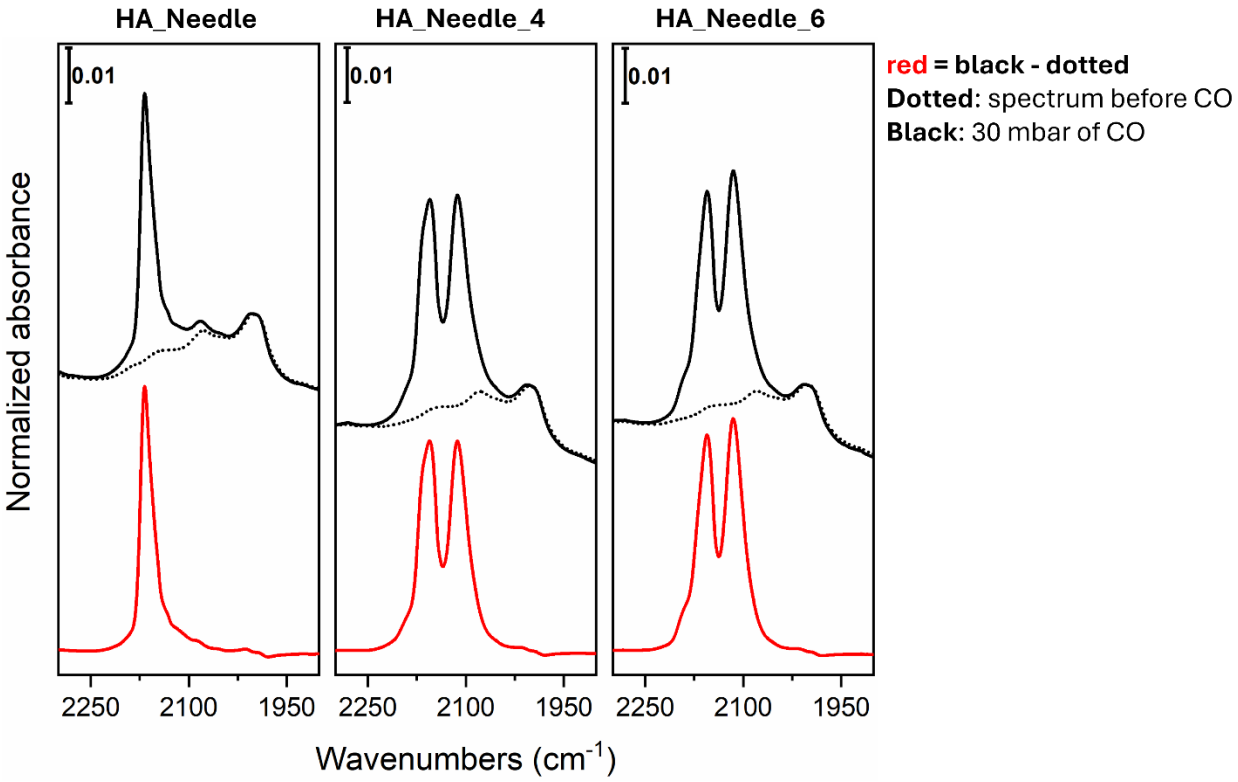

Figure S2. Comparison of the IR spectra at the highest CO coverage (P_{CO} = 30 mbar) for the different HA Needle samples. The data processing procedure used to obtain the spectra reported in Figure 4 of the main text is also shown: this includes the subtraction of the spectrum recorded before CO introduction (dotted lines) from the spectrum after CO admission (black lines) to obtain the final subtracted spectrum (red lines).

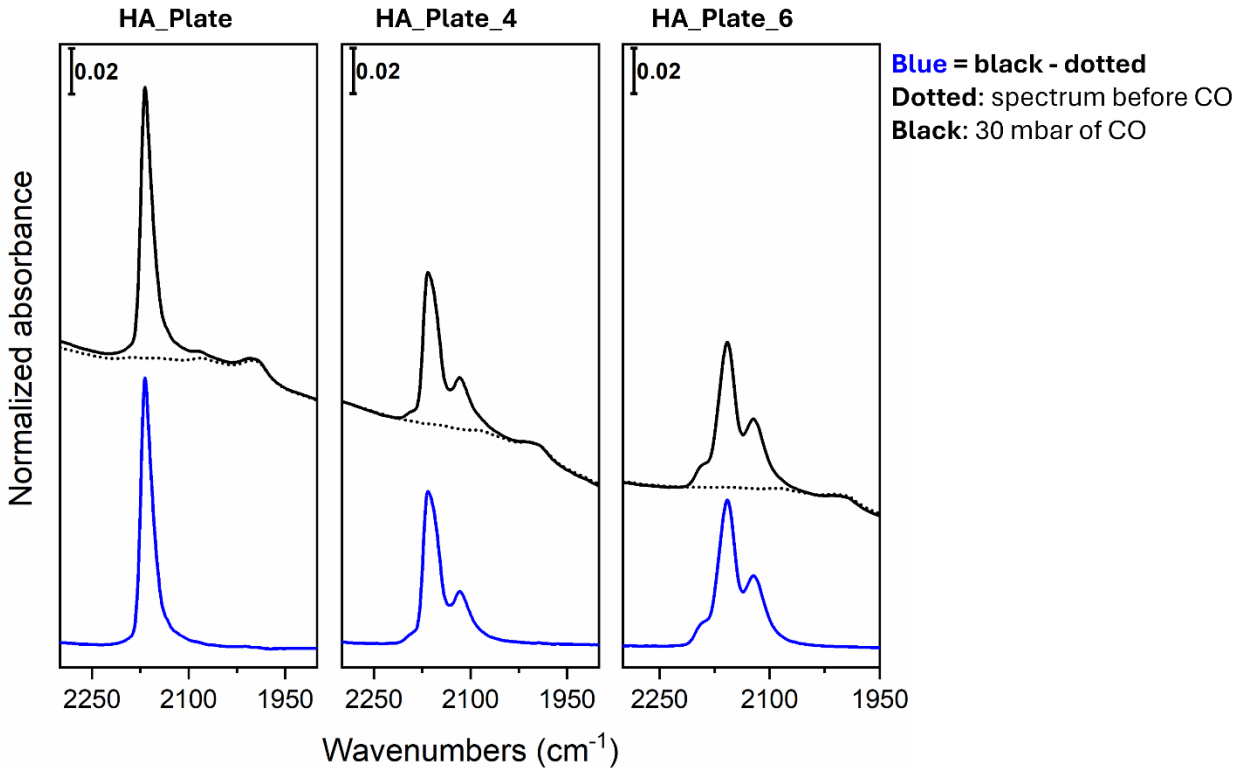

Figure S3. Comparison of the IR spectra at the highest CO coverage (P_{CO} = 30 mbar) for the different HA Plate samples. The data processing procedure used to obtain the spectra reported in Figure 4 of the main text is also shown: this includes the subtraction of the spectrum recorded before CO introduction (dotted lines) from the spectrum after CO admission (black lines) to obtain the final subtracted spectrum (blue lines).

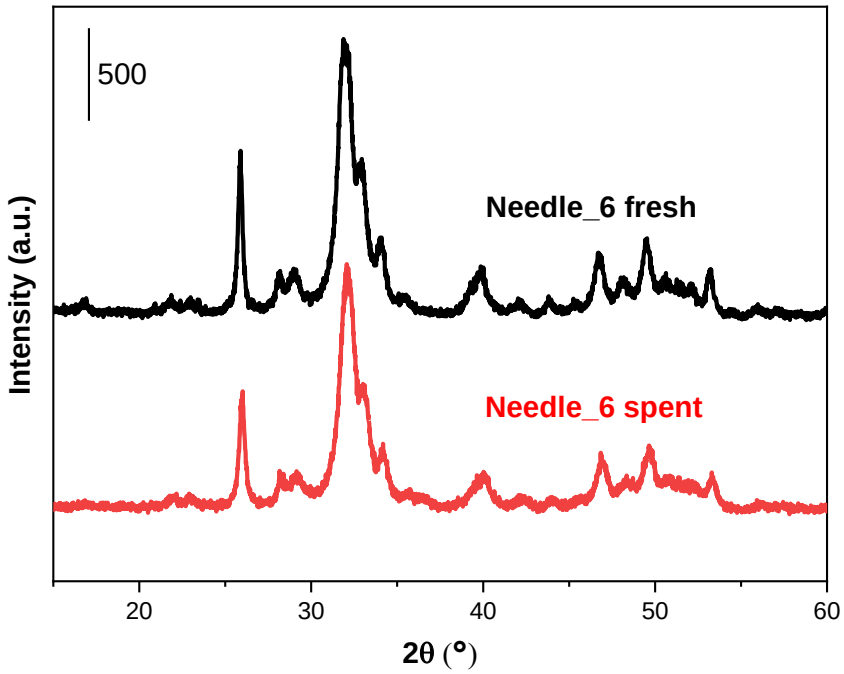

Figure S4. XRD patterns for fresh (as prepared) and spent (after catalytic tests) Needle_6 samples.

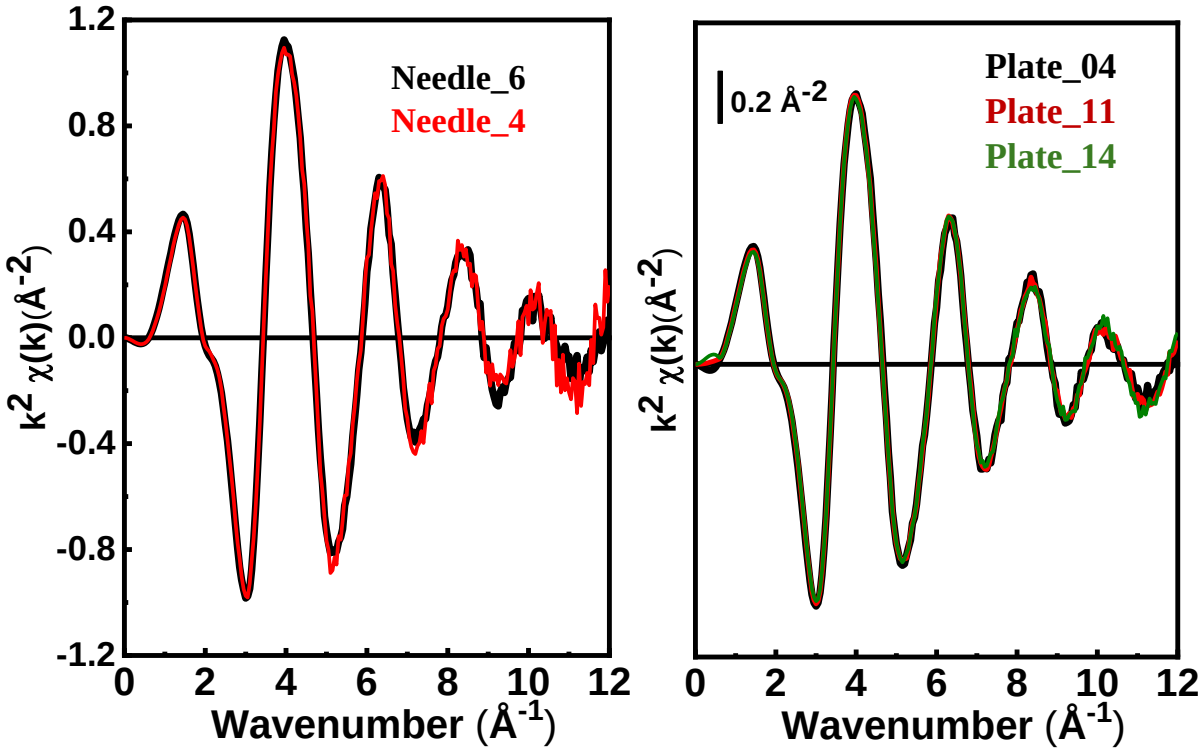

Figure S5. Cu K-edge k^2-weighted $\chi(k)$ spectra recorded for Needle and Plate HA samples with various copper loadings.

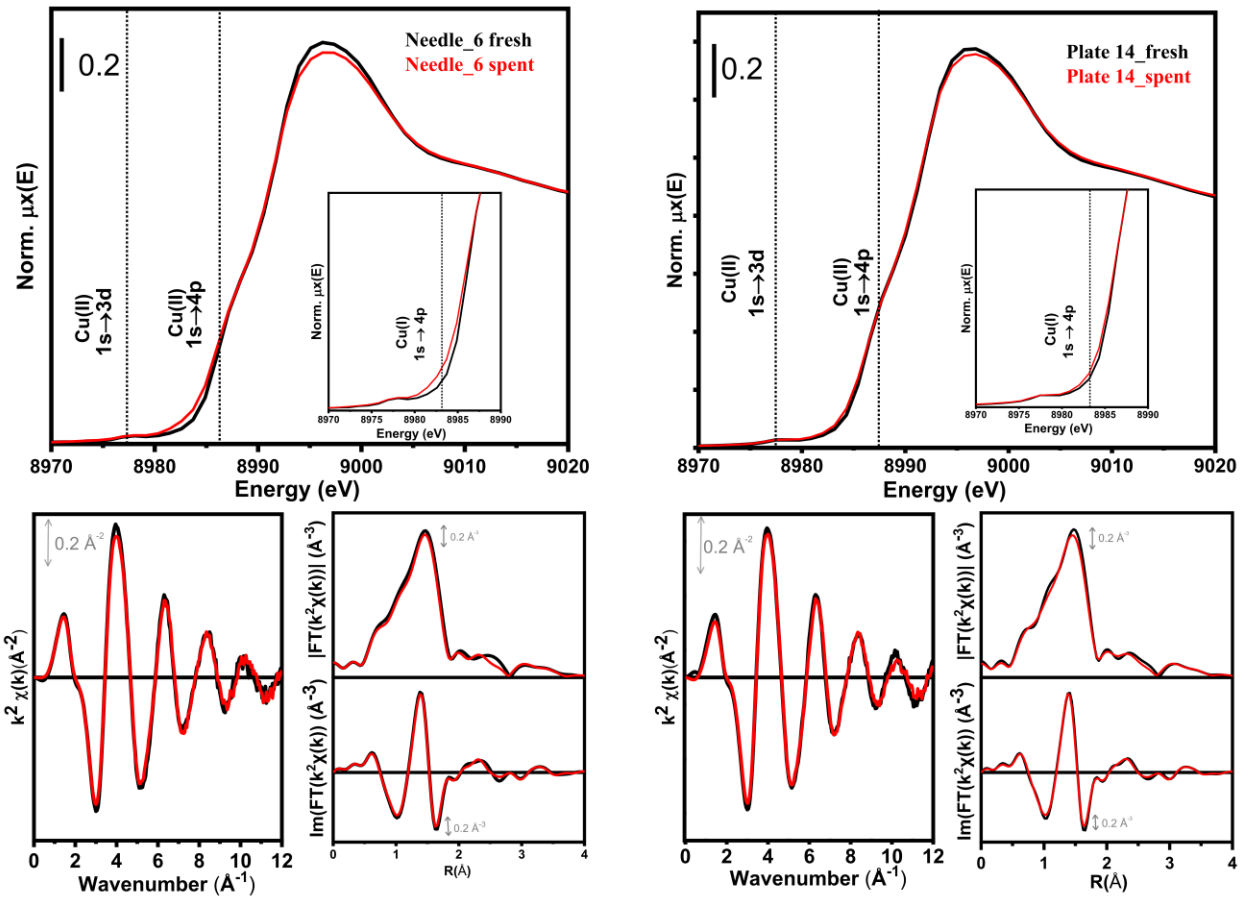

Figure S6. Top panel: Cu K-edge XANES spectra for fresh (as prepared) and spent (after catalytic tests) Needle_6 and Plate_14 samples. The insets show a magnification of the pre-edge region. Bottom panel: k^2-weighted $\chi(k)$ signal, magnitude and imaginary part of the phase-uncorrected Fourier transform of the k^2-weighted $\chi(k)$ signal in the 2.2–11.8 Å^{-1} range. Black lines represent the fresh catalysts and red lines the spent ones.

XANES Linear Combination Fit (LCF) procedure and results

In order to estimate the Cu(II) and Cu(I) fractions in selected fresh and spent samples, we applied XANES LCF, employing the Athena software.[1] As reference compounds, after considering different options, we selected $Cu_2CO_3(OH)_2$ (malachite) for the Cu(II) (dominant) component and Cu_2O as reference for the Cu(I) (minority) component. Indeed, as it can be noted in Figure S7, the line shape of the experimental XANES is significantly closer to $Cu_2CO_3(OH)_2$ (malachite) than to CuO, likely due to a similar coordination geometry on the Cu(II) centers. As for the Cu(I) component, reference spectra of CuCl and Cu_2S were excluded, due to the presence of characteristic, high-intensity, resonances in the rising-edge region, which are not observed in our experimental spectra.

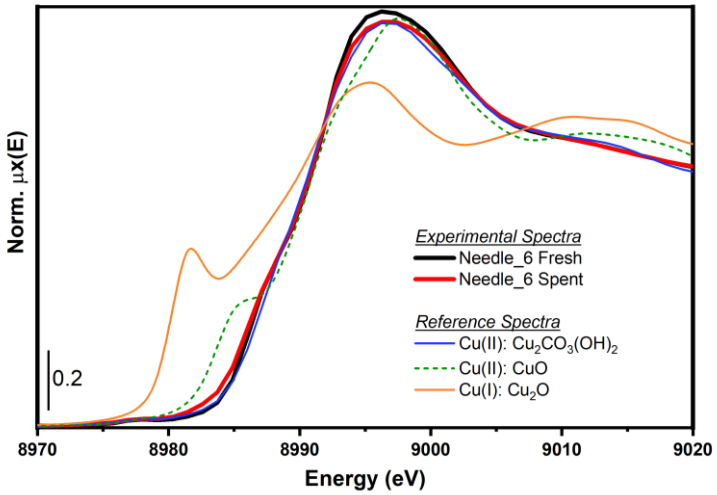

Figure S7. Comparison of representative Cu K-edge XANES spectra of a fresh and spent sample with possible reference spectra to be employed for LCF analysis.

After careful energy alignment and normalization of experimental and reference XANES spectra, we fitted each experimental XANES, $\mu^{EXP}(E)$, as a linear combination of the two reference spectra, $\mu^{REF}{}_i(E)$, *i.e.*: $\mu^{LCF}(E) = \Sigma_i w_i \mu^{REF}{}_i(E) = w_{Cu(II)} \mu^{REF}{}_{Cu(II)}(E) + w_{Cu(I)} \mu^{REF}{}_{Cu(I)}(E)$, optimizing the weights w_i for each reference spectrum. The LCF analysis was conducted by constraining the weights w_i to vary in the [0;1] range, while their sum $\Sigma_i w_i$ was not constrained to 1 and checked *a posteriori* for being compatible with unity within LCF errors, as an additional indicator of the fit reliability.

The LCF results for samples Needle_6 and Plate_14, in their fresh and spent state, are shown in Figure S8, Figure S9 and Table S2.

As expected from qualitative analysis of the experimental spectra, in both the fresh samples, the Cu(II) component is largely dominant, accounting virtually for 100% total Cu within the LCF error. In the case of spent samples, Needle_6 shows a minor, but still significant within the LCF error, Cu(I) contribution, accounting for ca. 3% total Cu. For Plate_14, although a slight increase

in the rising-edge region diagnostic of Cu(I) transitions and decrease of the white-line peak are qualitatively observed, the Cu(I) fraction determined by LCF is of 1%, within the fitting errors. To better discriminate and quantify such a minor contribution, the use of reference spectra accurately reproducing the coordination geometry and environment of Cu species present in the sample would be greatly helpful, although difficulty achievable with experimental spectra of model compounds.

Future *in situ* experiments are envisaged where Multivariate Curve Resolution (MCR) approaches[2] could be used on larger dataset to self-model from the dataset itself the pure spectra of Cu(II)(Cu(I) species formed in the investigated samples under reaction conditions.

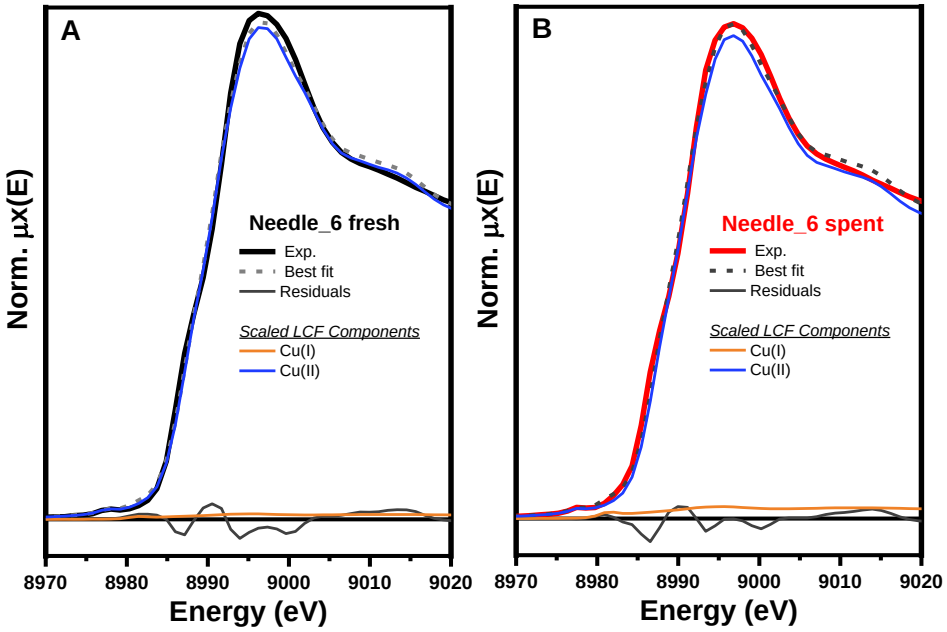

Figure S8. Comparison between experimental XANES spectra of sample Needle_6 and correspondent best-fit curves $\mu^{LCF}(E) = \Sigma_i w_i \mu^{REF}{}_{,i}(E)$ from LCF analysis. For each fitted spectrum, the Cu(II) and Cu(I) components scaled by their respective optimized weights and the LCF residuals are also reported.

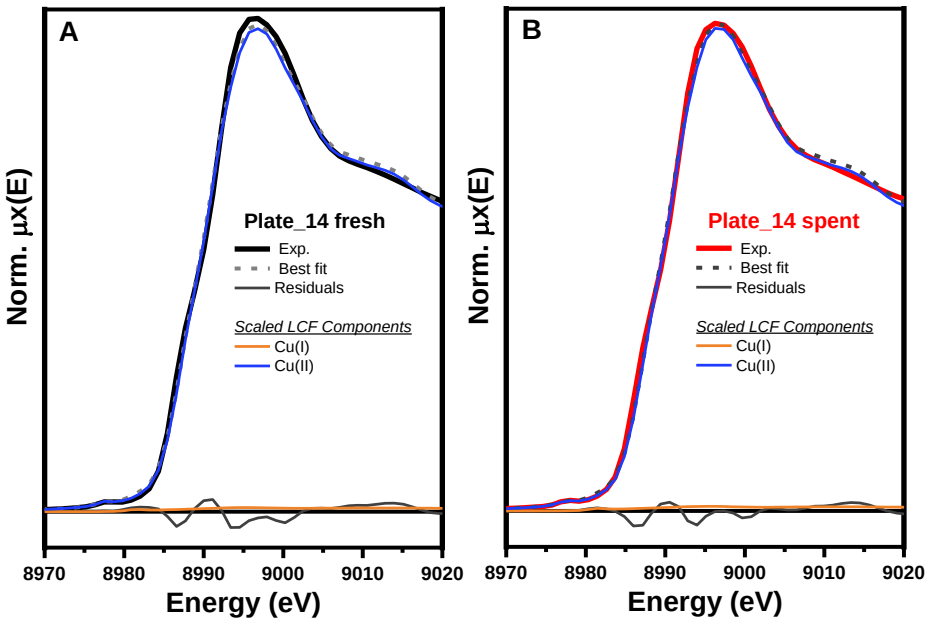

Figure S9. Comparison between experimental XANES spectra of sample Plate_14 and correspondent best-fit curves $\mu^{LCF}(E) = \Sigma_i w_i \mu_{REF,i}(E)$ from LCF analysis. For each fitted spectrum, the Cu(II) and Cu(I) components scaled by their respective optimized weights and the LCF residuals are also reported.

Table S2. Quantitative results of LCF analysis on XANES spectra for samples Needle_6 and Plate_14, in their fresh and spent state. R-factors are obtained as $\Sigma_j [\mu^{EXP}{}_j(E) - \mu^{LCF}{}_j(E)]^2 / \Sigma_j [\mu^{EXP}{}_j(E)]^2$, where j denotes each experimental point in fitted energy range, (8970 − 9020) eV.

Sample	R-factor	$w_{Cu(II)}$ Reference: $Cu_2CO_3(OH)_2$	$w_{Cu(I)}$ Referece: Cu_2O	$\Sigma_i w_i$
Needle_6 Fresh	0.0021	1.00 ± 0.01	0.01 ± 0.01	1.01
Needle_6 Spent	0.0016	0.98 ± 0.01	0.03 ±0.01	1.01
Plate_14 Fresh	0.0016	1.00 ± 0.01	0.01 ± 0.01	1.01
Plate_14 Spent	0.0011	1.00 ± 0.01	0.01 ± 0.01	1.01

References

1. B. Ravel and M. Newville, *J. Synchrotron Radiat.*, 2005, **12**, 537-541.
2. A, Martini, E. Borfecchia, *Crystals,* 2020, **10**, 664